DIRECTIONAL WAVE OBSERVATIONS IN CURRITUCK SOUND, NORTH CAROLINA

C. E. Long and D. T. Resio

U. S. Army Engineer Research and Development Center
Waterways Experiment Station
Vicksburg, Mississippi, USA

1. INTRODUCTION

Governing evolution of a wind wave field are at least the net effects of energy input from the wind S_{in}, the conservative rearrangement of energy among wave numbers k and directions q of the two-dimensional wave spectrum $F(k,q)$ by non-linear wave interactions S_{nl}, and losses by dissipative processes S_{ds}. Each of these source terms involves some very complicated physics in an environment where requisite detailed measurements are extremely difficult to make. Conventional wave measurements provide only indirect clues as to the nature of S_{in} and S_{ds}, and energy fluxes owing to S_{nl} tend to confound interpretation of such observations. Consequently, modeling characterizations of S_{in} and S_{ds} are subjects of ongoing research. Fortunately, theoretical considerations by Hasselmann (1961), Zakharov and Filonenko (1966), Webb (1978), Herterich and Hasselmann (1980) and others, in conjunction with an efficient computational algorithm by Tracy and Resio (1982) enable us to explore the nature of S_{nl} in great detail. Thus, if we acquire sufficiently detailed conventional wave measurements in a broad enough variety of environments, we can compute the effect of S_{nl} directly, and thereby deduce some of the effects of at least the sum of the remaining source terms, if not their individual contributions. Here, we describe an initial step in this approach, the acquisition and preliminary statistical reduction of frequency-direction spectra of small waves in a shallow, enclosed basin.

2. MOTIVATION FOR AN EXPERIMENT

An important part of the wave spectrum is the equilibrium range of wave numbers, where, under reasonably steady winds, the net effect of the sum of source terms yields a one-dimensional spectrum $F(k)$ that scales simply with gravitational acceleration g and a velocity parameter u that is related to the wind. Scaling arguments by Toba (1972), Kitaigorodskii (1983) and Resio (1987), observations by Toba (1973), Mitsuyasu (1980), Forrestall (1981) and Donelan, et al. (1985), and studies using the numerical form of S_{nl} by Resio and Perrie (1991) and Resio et al. (2001) provide compelling arguments for an equilibrium-range spectrum of the form

$$F(k) = b\,k^{-5/2}, \qquad (1)$$

where b is given (from scaling alone) by

$$b = \tfrac{1}{2} a\, u g^{-1/2}. \qquad (2)$$

With a proper choice of u, the dimensionless coefficient a is constant. The wave number span of the equilibrium range corresponds to cyclic frequency f roughly satisfying $1.5 f_p < f < 3 f_p$, where f_p is spectral peak frequency, and, using linear dispersion, $4\pi^2 f^2 = gk\tanh kh$, where h is water depth. Note that the one-dimensional frequency spectrum $E(f)$ is related to $F(k)$ by $E(f) = \frac{2\pi}{c_g} F(k)$, where c_g is group velocity. The form of (2) in combination with (1) then leads (in deep water) to

$$E(f) = \frac{2}{(2\pi)^3} g^{3/2} b\, f^{-4} = \frac{a}{(2\pi)^3} u g f^{-4}, \qquad (3)$$

which is a form commonly used with measured spectra.

In work leading to the paper by Resio, et al. (2004), the present authors sought an appropriate expression for u in (2) that yielded a reasonably constant a in observed $F(k)$ spanning a wide range of scales. In the initial stages of that work, data from two gauges at the U.S. Army Engineer Research and Development Center Field Research Facility (FRF) on the northern Outer Banks of North Carolina provided estimates of b for ocean waves. Fig. 1 shows the locations of these gauges. Gauge 630 is a Waverider buoy located about 6 km from shore in about 21 m water depth. Gauge 625 is a Baylor gauge (a surface-piercing, impedance-type wave gauge) suspended beneath the seaward end of a pier that extends about 0.5 km from shore in a local (pier-scoured) depth of about 8 m. Data from Lake George, Australia (Babanin, et al. 2001 (with a representative set of $E(f)$ kindly provided by those authors) enabled estimates of b from a bounded water body having much smaller scales than those of the FRF data. Water depths at the measurement site about 50 m from the east shore of Lake George ranged from 0.6 m to 1.1 m in data shown here.

Estimates of b arise simply from observed wave spectra with an average given by

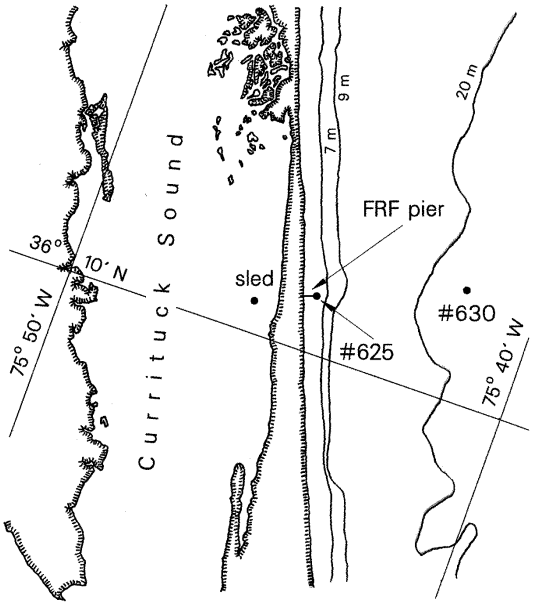

Fig. 1. Site map of FRF and vicinity.

$$b = \left\langle k^{5/2} F(k) \right\rangle_{f_1}^{f_2} , \qquad (4)$$

where f_1 and f_2 are bounding frequencies appropriate to an equilibrium range. For the FRF 630, we used the conventional $f_1 = 1.5 f_p$ and $f_2 = 3 f_p$. For both FRF 625 and Lake George, there was increased energy near $2 f_p$, suggesting shoaling effects that would bias b estimates, so the frequency range for (4) was adjusted so that $f_1 = 2.5 f_p$ and f_2 was the highest sampled frequency that was free of possible capillary effects (0.5 Hz for FRF 625 and 5 Hz for Lake George).

Correlating velocity scales for use in (2) included friction velocity u_*, wind speed at 10 m elevation u_{10}, and, following Resio, et al. (1999), wind speed u_l at an elevation equal to a fixed fraction l ($= 0.065$) of the spectral peak wavelength. All winds were assumed to follow a neutrally stratified logarithmic profile having a von Karman coefficient $k = 0.41$ and subject to a Charnock (1955) surface roughness $z_0 = \alpha_c u_*^2 / g$ with $\alpha_c = 0.015$. Thus,

$$u_l = \frac{u_*}{k} \ln \frac{2\pi l g}{\alpha_c u_*^2 k_p} , \qquad (5)$$

where k_p is spectral peak wave number.

Correlation of estimated b from the three data sources with velocity scales u_*, u_{10} and u_l yielded the highest correlation coefficient r^2 when we used u_l. That correlation is shown in Fig. 2, which shows that while the ocean data follow the correlation line with some consistency, the Lake George data deviate in a clearly systematic way. This result suggests at least three possibilities: the best of our three candidate velocity scales does not apply to small-scale waves, our method for estimating b from Lake George data is incorrect, or the Lake George environment does not yield waves that conform to the model expressed by (1) and (2).

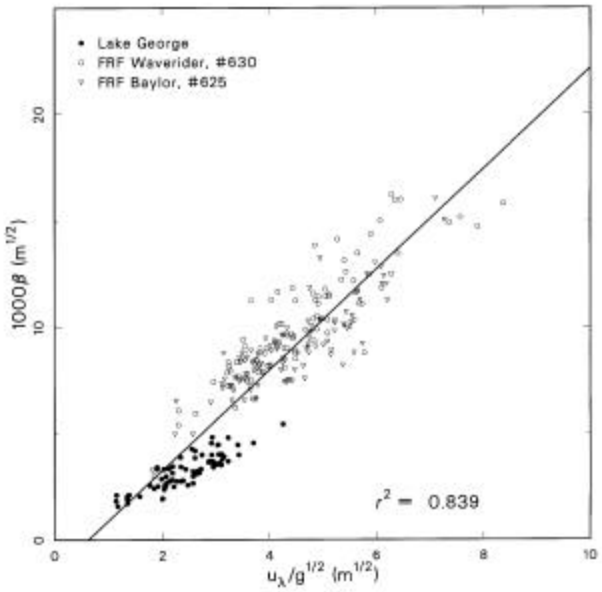

Fig. 2. Preliminary correlation of b with u_l, showing the difference of Lake George from ocean results.

To test these hypotheses, we needed data from another source with an environment like that of Lake George. Lacking such data, we were motivated to conduct a new investigation. A description of the resulting experiment is the subject of this paper, but we note here that wind data and $F(k)$ were acquired and b were estimated from those data using (4) for frequencies in the range $1.5 f_p$ to $3 f_p$. A correlation with u_l, like that shown in Fig. 2, revealed a behavior very much like that of the Lake George data, and likewise not in good agreement with data from the other sources.

Subsequently, it was realized that the similarity and scaling arguments given by Resio and Perrie (1989) would better suffice to link the wide range of scales represented by the collective data sets. Resio and Perrie (1989) deduce that a velocity scale for the flux of *energy* from air to water is more appropriately expressed as $\left(u_*^2 c_p\right)^{1/3}$, where c_p is spectral peak phase speed and serves to act as a scale for wave phase speeds in the vicinity of the spectral peak.

Generalization of the velocity scale suggests that forms like $\left(u_{10}^2 c_p\right)^{1/3}$ and $\left(u_l^2 c_p\right)^{1/3}$ may also apply. Correlations of estimated b with velocity scales $\left(u_*^2 c_p\right)^{1/3}$, $\left(u_{10}^2 c_p\right)^{1/3}$ and $\left(u_l^2 c_p\right)^{1/3}$ all yielded similar results with correlation coefficients much higher than that shown in Fig. 2. The best overall characterization of the data employed the scale $\left(u_l^2 c_p\right)^{1/3}$. Fig. 3 shows a correlation between $\left(u_l^2 c_p\right)^{1/3}$ and b for the three data sets shown in Fig. 2 plus the data described in this paper and data from two National Data Buoy Center (NDBC) platforms (41001 in the western North Atlantic ocean and 46035 in the Bering Sea).

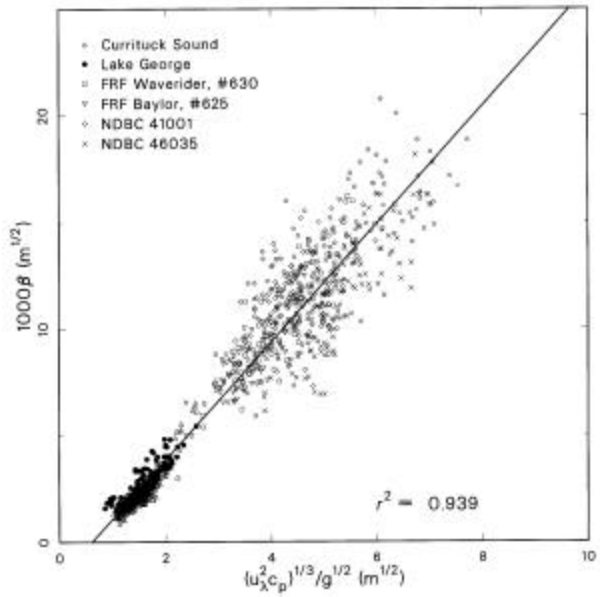

Fig. 3. Correlation of b with $\left(u_l^2 c_p\right)^{1/3}$ using data from six disparate sites.

The broad range of scales represented in Fig. 3, the relatively high r^2 and the lack of obvious systematic deviation by any of the data suggest that $\left(u_l^2 c_p\right)^{1/3}$ is a reasonable velocity scale for the equilibrium range. From the parameters of the regression line in Fig. 3, a model for b takes the form

$$b = \tfrac{1}{2} a \left[\left(u_l^2 c_p\right)^{1/3} - u_0\right] g^{-1/2}, \qquad (6)$$

with $a = 0.00553$ and $u_0 = 1.92$ m/s. This model is useful in some aspects of data interpretation.

The existence of the offset velocity u_0 in (6) is a consequence of our regression and is, at this point, a curiosity. Under simpler scaling arguments, one might expect u_0 to have a value near zero, which would imply that our non-zero value owes to some form of error. However, common sources of error do not appear capable of reducing u_0 to zero. If surface drift is considered and that drift is roughly 1 to 3 times u_*, then u_* would have to be between 0.6 m/s and 1.9 m/s, which is not the case for these data. If Doppler effects owing to following currents are important, our estimates of b would tend to be too high, and correcting b would tend to increase u_0, not reduce it. If atmospheric stability is relevant, our estimates of u_* would have to be high by a factor of up to about 2 for the small scale data. Such a situation would require stable stratification for all data, which does not seem likely.

At face value, (6) indicates that the scale for the equilibrium range goes to zero at a finite wind speed. In combination with (1), this suggests there is no energy at conventional equilibrium-range frequencies, an unlikely situation. However, the small-b situation may be legitimate in the sense of numerical work by Resio, et al. (2001), where those authors show that, owing to S_{nl} alone, the net flux of energy from the spectral peak region to higher frequencies is essentially proportional to b^3. Where b approaches zero, the net non-linear flux to higher frequencies may likewise go to zero, or even reverse. In the absence or reversal of this flux, an equilibrium range may not exist. There would still be energy at the conventional equilibrium-range frequencies, but it would arise from a combination of source terms that would lead to a form of scaling different from (but at some level asymptotic to) Eq. (6). As suggested by Fig. 3, this behavior would occur for waves at scales smaller than the smallest waves considered here, i.e., probably during the very initial stages of wave growth. However, the resulting offset velocity u_0 appears to apply to waves of all scales, and so may be an important general consideration in wave modeling.

3. EXPERIMENT DESCRIPTION

Our experiment was somewhat *ad hoc* when judged from a broad view. Our immediate needs, which we achieved, were to obtain simple wind and wave data at a site comparable to Lake George. However, logistical constraints prevented direct measurements of wind stress, atmospheric stability, local mean currents and a complete bathymetric survey of the experiment site. Thus, the experiment was somewhat incomplete, and there may be reasonable concerns about interpretation of results. On the other hand, where it was necessary to deploy at least one wave gauge with which to estimate $F(k)$, it was relatively straightforward to deploy an array of gauges so as to obtain estimates of $F(k,q)$. With some care in interpretation, these observations may provide considerable insight into directional wave behavior.

3.1 Site

The experiment site was Currituck Sound, North Carolina (Fig. 1), chosen for its very practical adjacency to our FRF home base and because waves evolving there are at scales much like those in Lake George. Currituck Sound is a body

of water elongated in the north-south direction, residing between the northern North Carolina Outer Banks and the mainland to the west. The nearest ocean inlet is about 40 km to the south, and except for an opening to the larger, deeper Albemarle Sound at its southern end, Currituck Sound is nearly landlocked. The dot marked "sled" in Fig. 1 indicates where we made our measurements. From that point, the shortest fetch to solid land is about 0.9 km to the east. In the westerly direction, the shortest fetch is about 5.5 km. To the northwest, the maximum fetch is about 14 km. A similar maximum fetch exists to the southwest, except for the roughly 25-degree arc of directions leading to Albemarle Sound, where the fetch is much greater.

Actual effective fetches in some directions are likely to be smaller than the maximum fetches just described. We were able to survey a small rectangular region, about 0.5 km by 3 km with the long axis oriented east-west, in the vicinity of the sled site. This survey showed a depth at the sled site of 2.2 m relative to the 1929 National Geodetic Vertical Datum with variations from 1.8 m to 2.4 m over most of the surveyed area, but with a steep bank about 0.5 km to the east of the sled and depths of about 0.6 m to the east of that point. We found that our survey did not agree in detail with the NOAA chart on which we had relied for basin bathymetry. That finding cast doubt on other details of the NOAA chart, and, unfortunately, we were not able to do more extensive surveying. The NOAA chart and local fishing lore indicate a channel several km wide with depths of 1.8 m to 2.1 m extending along the long axis of Currituck Sound in the vicinity of the FRF, and we assumed this was the case. The same sources suggest many shoal areas within a few km to the north and south of our site, but we do not know details of their sizes and locations. These features would likely limit the effective fetch for waves at our site.

This situation is not critical for our basic purpose. We can reasonably assume that for winds generally from the west, there is sufficient fetch over water of sufficient depth that we can relate local wind scales to local wave spectra with some confidence. What we cannot do is test any fetch-growth hypotheses.

3.2 Sensor Platform

The instrumentation in our experiment essentially consisted of a directional wave gauge and an anemometer mounted on a sled. Fig. 4 shows some of the basic parts of the sensor platform in its deployed position. A three-legged pipe-frame tower with a working stage near its top held a solar panel and battery box to provide electrical power, a weatherproof box housing a multiplexer and radio transmitter that sent data to the FRF main building via an antenna (on the short mast above the handrail), a lightning rod (on the tall mast), and an anemometer (R. M. Young model 09101 digital wind speed and direction) on the third mast.

The directional wave gauge consisted of an array of nine capacitance-type wave rods of 0.6-mm diameter and 3-m length (Ocean Sensor Systems, Coral Springs, Florida) with

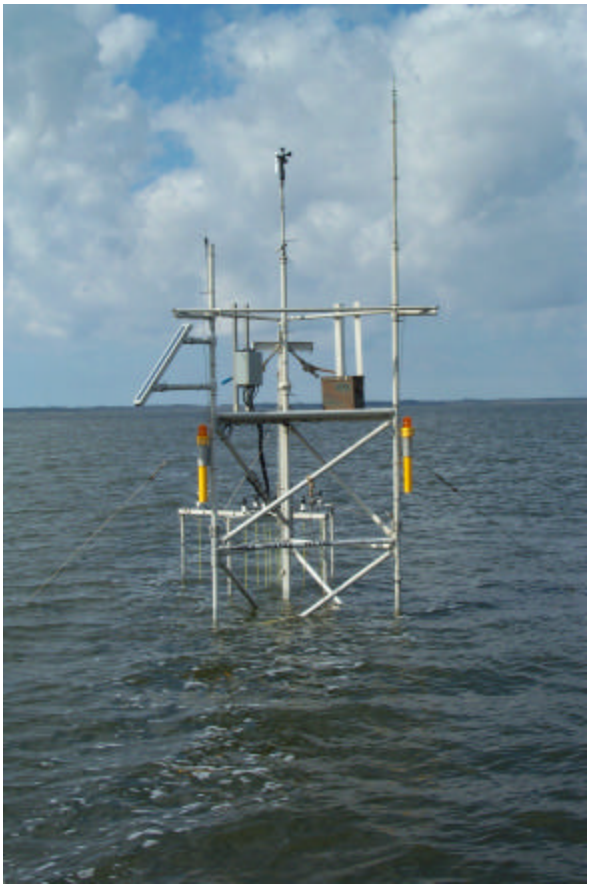

Fig. 4. Instrument platform used in Currituck Sound.

internal digitization of water levels into 4,096 steps along the sensor length. A gauge cage (seen on the far side of the pipe tower in Fig. 4), consisting of two horizontal cruciform frames separated in the vertical by pipes at the frame ends, held the array of wave rods. The wave rods were not rigid and, if not constrained, would tend to flex under wave action. This behavior would compromise the necessary fixed relative spacing of the wave rods, so a set of horizontal stays (made of fishing line) tied the wave rods in their requisite geometric pattern to the vertical pipes of the gauge cage.

Fig. 5 shows the geometry of the directional array. It has the form of two orthogonal linear arrays with one shared gauge. The two-dimensional character of this array allows full 360-degree directional resolution, and avoids the 180-degree ambiguity that plagues one-dimensional arrays. The design of each linear-array arm follows the guidance given by Davis and Regier (1977). Minimum gauge spacing is 0.1 m, which means that the shortest resolvable wave must have a length in excess of 0.2 m, or, in deep water, a frequency less than about 2.8 Hz. Maximum gauge spacing (along one arm, a degenerate case for wave crests parallel to that arm) is 1.6 m. Reasonably detailed directional resolution is possible for waves several times this length because directional estimates are based on cross-spectral phase differences between pairs of gauges and the array needs only

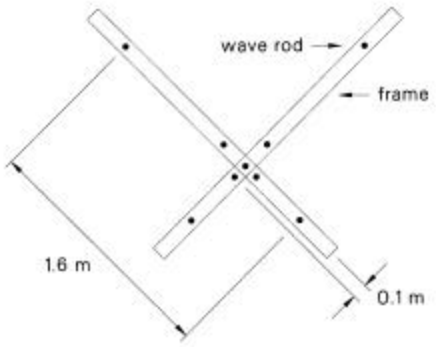

Fig. 5. Dimensions and pattern of the Currituck Sound directional wave array.

sample a large enough fraction of a wave length to detect a phase difference. Beyond about ten times maximum spacing (a wave length of about 16 m or a deep-water frequency of about 0.3 Hz), resolution degrades to that of a low-resolution directional gauge, capable of estimating only a few of the low moments of a directional distribution function. However, the range of frequencies from 0.3 Hz to 2.8 Hz includes the frequencies of interest in this study, so the array geometry is adequate for our purposes.

Prior to deployment, each of the wave rods was statically calibrated along its sensing length to establish a gain and offset for interpretation of its digital output. With the exception of a few tens of cm at the tops and bottoms of the wave rods, the response was very linear. For the central 2 m of the working length, all of the calibrations had a correlation coefficient $r^2 > 0.99993$.

3.3 Sampling Pattern and Data Analysis

The sled was deployed at the location shown in Fig. 1 from 24 October 2001 to 19 April 2002. A data collection began at the top of every hour and lasted for about 41 minutes. The wave gauges were sampled synchronously at time steps of 0.2048 s (about 4.88 Hz) so that each gauge had a record of 12,288 readings. The 2.44-Hz Nyquist frequency was thus compatible with the geometry of the directional array. Fourier analysis with segment and band averaging yielded auto- and cross-spectra at frequency increments of about 0.024 Hz, each having 120 degrees of freedom. Auto-spectra from the nine sensors were averaged to produce an estimate of the total variance at each frequency $E_T(f)$. These variances were filtered based on directional considerations described in Section 3.6 to provide final estimates of the one-dimensional spectra $E(f)$. The transformation

$$F(k) = \frac{c_g}{2p} E(f) \tag{7}$$

provided estimates of one-dimensional wave number spectra.

The iterative maximum likelihood estimator (IMLE) of Pawka (1983) (adapted to a two-dimensional array) provided direct estimates of directional distribution functions $D(f,q)$, which, in combination with $E_T(f)$, yield estimates of frequency-direction spectra $E(f,q)$ by the conventional expression

$$E(f,q) = E_T(f) D(f,q). \tag{8}$$

Estimates of wave number-direction spectra are then

$$F(k,q) = \frac{c_g}{2p} E(f,q) \tag{9}$$

by virtue of (7) and linear dispersion. Note that here we use rectangular rather than polar coordinates to express the directional distribution function so that

$$\int_0^{360} D(f,q)\, dq = 1. \tag{10}$$

The IMLE scheme assumes that the amplitude of a wave at a particular frequency and from a particular direction can be modeled as a linear combination of the Fourier components at that frequency from the sensors in a spatial array of gauges. The method is entirely consistent with linear wave theory, and where that theory is valid, the IMLE is valid. Extensive numerical testing of a six-element array on Harvest Platform near Point Conception, California, by Long (1995) and of a fifteen-element array at the FRF (unpublished) indicate that the method is quite accurate in recovering a specified directional distribution from its associated Fourier representation, even in the presence of moderate noise. However, the method is just an estimator, based on sparse sampling, and there is no ground truth, so results must be interpreted as an indication of, rather than absolute, truth.

We did not use all gauges shown in Fig. 5 in directional estimation at all frequencies. For example, we did not use the outermost gauges of the array for high-frequency calculations because natural waves tend to become uncorrelated at scales of about three wavelengths. Cross-spectra across the outer span of the array would then be very noisy and thus compromise directional estimates. We did not use closely spaced gauges for low-frequency calculations because such gauge pairs do not resolve well the phase differences of long waves. For all but the very lowest frequencies, we used at least five gauges. A simple rule of thumb is that a circle divided by the number of independent measured cross-spectral elements gives an arc at which two directional peaks can be resolved. With five gauges, that arc is about 18 degrees. To resolve such potential peaks, we set our algorithm to make estimates at 2-degree increments.

We deployed the wind sensor as it came from the manufacturer, without independent calibration (beyond a few coarse field tests). Anemometer speed and direction

had 1-Hz sampling, and these data were vector averaged for the duration of a collection to characterize local winds.

3.4 Initial Quality Control

Though we collected several thousand spectra during the sled deployment, there were two characteristics of our system that decimated considerably the number of useful results (beyond an occasional dead battery and infrequent fouling of the array by drifting plants). One was the discrete sampling step of our wave rods. The other was an effect of the horizontal stays employed to stabilize the array.

The least-significant-bit chatter of the wave rod output digitizers established a computable (white) noise floor that was significant relative to spectral densities at high frequencies in our low-energy observations. In the paper by Resio, et al. (2004), which examined spectral levels at equilibrium-range frequencies, we eliminated all collections with $u_{10} <$ 5 m/s and $f_p >$ 0.7 Hz to avoid the noise floor problem in an indirect way. In the present paper, we are interested in high-frequency information, so, in addition to the previous constraints, we eliminate the parts of any spectrum having $E(f)$ less than ten times the noise floor. This has the effect of truncating the high-frequency parts of low-energy spectra, but helps avoid a known source of noise.

The horizontal stays performed their design function very well, and gave no problem as long as they were either completely submerged or completely sub-aerial. However, when they intersected the water surface, they gave rise to impedance paths with which the wave rod circuitry could not deal, and wave signals were seriously distorted. Because this condition was more prevalent in high waves, we lost some very interesting high-energy observations. Fortunately, the effect was very obvious in processed results, so we were easily able to avoid compromised data.

3.5 Example Spectrum

Fig. 6 illustrates one example of the set of $E(f,q)$ arising from the Currituck Sound measurement campaign. It has several interesting features, including a single sharp peak, a suggestion of a directionally bimodal high-frequency tail, and no clear evidence of waves from extraneous sources (i.e., swell). We will examine details of this and other spectra in Sections 4 and 5, but Fig. 6 with Fig. 1 helps define the coordinate system used here. Our x-axis begins at the sled and is directed toward magnetic east, being roughly normal to the long axis of Currituck Sound. The y-axis is directed toward magnetic north. Directions are defined in the geometric (rather than a geophysical) sense, and increase counter-clockwise from the x-axis. Thus, +90 deg represents magnetic north, -90 deg is magnetic south, and $\pm$ 180 deg is magnetic west. Both winds and waves are given in the 'from' sense, so that the wind and waves illustrated in Fig. 6 are from the southwest.

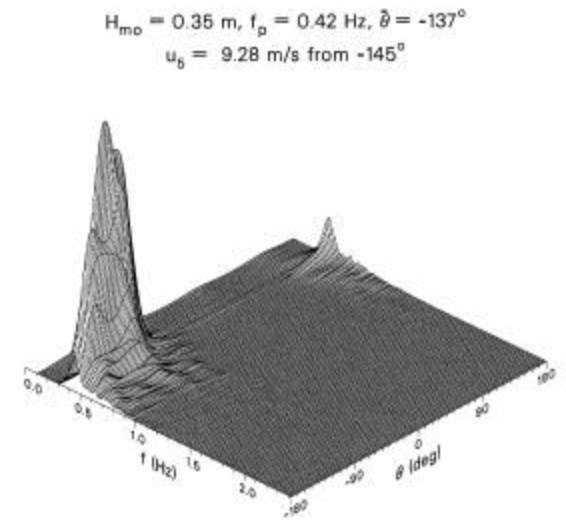

Fig. 6. An example frequency-direction spectrum from Currituck Sound.

3.6 Additional Constraints

There were 1614 observation cases remaining after the initial screening described in Section 3.4. To help ensure that wind and wave scales are compatible, we decimate the data set further based on the following considerations.

As noted in Section 3.1, we do not know enough about effective fetches in Currituck Sound to test fetch-growth hypotheses, but we can do an inverse analysis by using a fetch-growth model to see if the evident origins of our data are compatible with extant basin boundaries. The model we use is an adaptation of an expression derived by Resio and Perrie (1989), taking the form

$$fetch = 431g\left(\frac{H_{mo}}{u_*}\right)^2, \qquad (11)$$

where H_{mo} is variance-based characteristic wave height. Fig. 7 shows as symbols estimated fetch as a function of wind direction q_w for our 1614 observations. The solid line in Fig. 7 is an estimate of absolute limiting fetch based on distance from the sled position to solid land along various possible wind azimuths. For winds generally from the north, west and south, waves evidently originate within the body of the sound, suggesting fetch- or duration-limited growth. Some offset from an upwind boundary is sensible for fetch-limited growth if one considers that it takes a distance of order 100 times the height of an upwind roughness element for a new internal boundary layer to form. Given the trees, dunes and houses with heights of order 10 m that line the boundaries of the sound, it may take about 1 km of open water for significant wave growth to begin. If significant shoals or transient winds exist, then evident fetches may be considerably closer than upwind solid land. One does not expect the fetch to exceed the limiting fetch, however. Many of the points from the northeast in Fig. 7 do exceed this limit, suggesting an

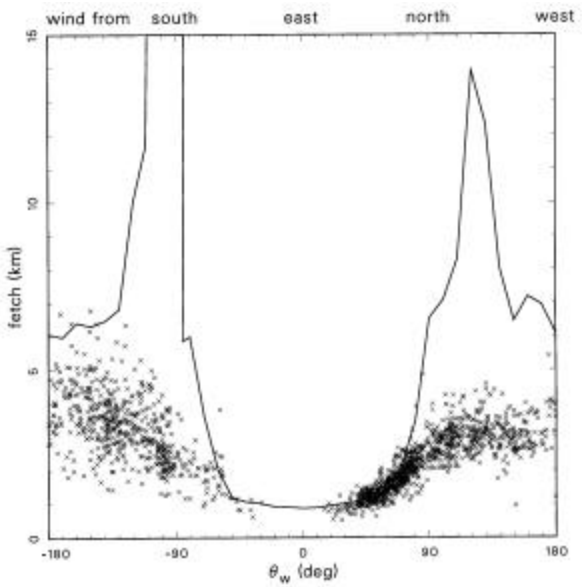

Fig. 7. Apparent (symbols) and limiting (solid line) fetches as functions of upwind azimuth for sled observations in Currituck Sound.

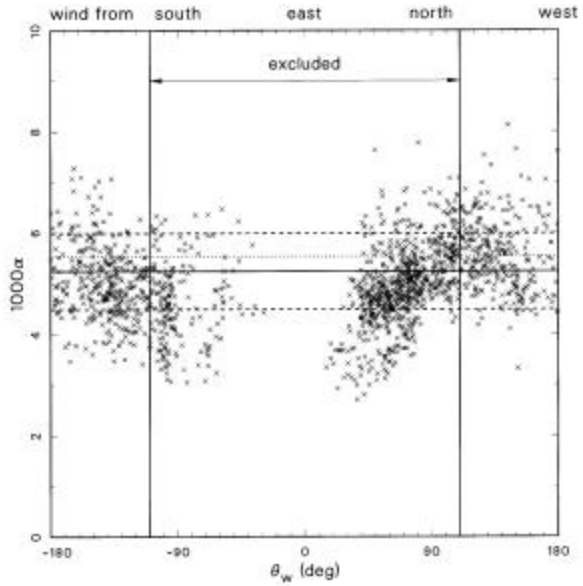

Fig. 8. Estimates of coefficient a in terms of upwind azimuth.

imbalance (in the similarity sense) between wind and waves over these short fetches and oblique wind directions.

This suggestion is supported by Fig. 8, which illustrates estimates of the coefficient a in (2) as a function of wind direction. Here we use our data to estimate b based on (4) (with frequency limits $f_1 = 1.5 f_p$ and $f_2 = 3 f_p$) and velocity scales given by (6), so that

$$a = \frac{2 b g^{1/2}}{\left(u_l^2 c_p\right)^{1/3} - u_0} \ , \qquad (12)$$

with u_l given by (5). Though there is some scatter of a estimates in Fig. 8, there is a distinct tendency toward lower values at directions associated with short fetches and oblique winds. While we can examine these cases in more detail at a later time, we retain for the present study only those cases for which the fetch to solid land was at least 5 km, which should allow enough space for (steady) wind and waves to reach some kind of dynamic balance. A conservative expression of this constraint is $|q_w| > 110$ deg. The vertical lines in Fig. 8 indicate the arc excluded by this constraint. With this constraint, there remain 649 observations for use in the present study. The bold horizontal line in Fig. 8 represents the mean a from these remaining observations. The dashed horizontal lines show one standard deviation on either side of this mean. The horizontal dotted line is the a deduced from six disparate data sets based on the regression shown in Fig. 3, which shows consistency between the Currituck Sound data and the more general data set (although the latter includes the former, so the two are not independent and some agreement is not surprising).

A final constraint on the data arises from evidence (shown in Section 5) of high-frequency waves propagating upwind, a condition we would not expect in open water. We ascribed these signals to wave reflections from submerged parts of the sled structure, which, owing to our directional constraint were generally downwind of the directional array. An advantage of directional measurements is that one can isolate downwind propagating waves. We did this by summing the downwind energy in each $E(f,q)$ to form an estimate of the relevant one-dimensional frequency spectra used in our subsequent analysis. The filter algorithm is

$$E(f) = \int_{q_w-90}^{q_w+90} E(f,q)\,dq = E_T(f) \int_{q_w-90}^{q_w+90} D(f,q)\,dq \ , \qquad (13)$$

where q_w is wind direction.

4. ONE-DIMENSIONAL SPECTRA

The 649 cases remaining after our various filters have ranges of bulk parameters listed in Table 1. Because our goal was to measure waves similar in scale to those in Lake George, Table 1 also shows ranges of parameters represented by data we used from that site. There is broad agreement between the two environments. There are higher peak frequencies in the Lake George set, and such conditions exist in Currituck Sound, but we lost our samples of such cases owing to the noise floor constraints described in Section 3. The main difference between the two sites is water depth. The shallower water of Lake George suggests that depth-related effects may be more prevalent in data from that site. Except for depth differences, the two sites have similar scales.

Table 1. Parameter Ranges Associated with Currituck Sound and Lake George Data.

	Currituck Sound	Lake George
cases	649	77
u_{10} (m/s)	5.0 – 15.7	5.1 – 19.8
H_{mo} (m)	0.09 – 0.59	0.05 – 0.44
f_p (Hz)	0.35 – 0.63	0.32 – 1.07
k_p (rad/m)	0.44 – 1.62	0.67 – 4.68
h (m)	2.28 – 2.93	0.60 – 1.15
$k_p h$	1.17 – 3.99	0.70 – 3.12
$H_{mo} k_p$	0.11 – 0.35	0.14 – 0.41
H_{mo}/h	0.04 – 0.22	0.09 – 0.39
u_{10}/c_p	1.46 – 4.09	2.13 – 6.65

4.1 Mean Normalized Spectra

To characterize the general character of the Currituck Sound observations, we normalize the one-dimensional wave-number spectra with equilibrium range scales and average the results from all 649 samples. From (1), spectra in the equilibrium range should behave as $bk^{-5/2}$, so that normalizing wave-number spectra as $k^{5/2}F(k)/b$ will yield unit value in any existing equilibrium range of k or its corresponding range of f. We further cast discrete normalized spectral elements into bins of f/f_p to examine spectral structure relative to its peak. Fig. 9 shows the means (symbols) and standard deviations (error bars) of the resulting bin contents.

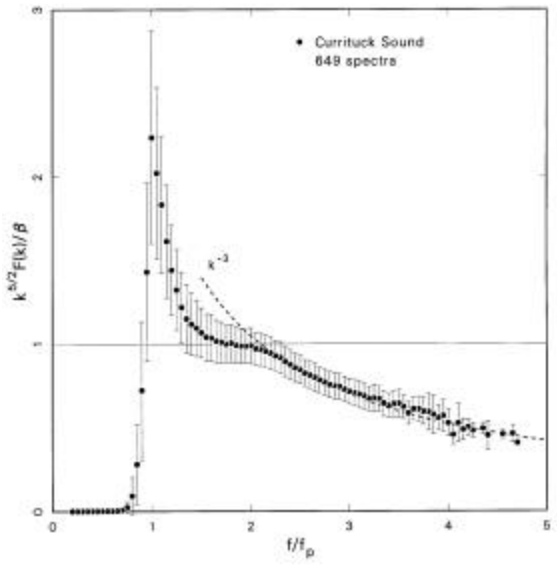

Fig. 9. Means (symbols) and standard deviations (error bars) of 649 equilibrium-range-normalized wave-number spectra in spectral-peak-relative frequency bins.

Fig. 9 has several interesting features. Spectral densities in the vicinity of the spectral peak have large standard deviations, suggesting variations in peak enhancement among members of this data set. The enhanced peak region terminates near 1.5 f_p, at which point the mean spectrum flattens, being roughly constant up to about 2.1 f_p. Beyond 2.1 f_p, the mean spectrum systematically falls below the constant line representing $k^{-5/2}$ behavior, and, indeed, appears quite consistent with a k^{-3} behavior (the dashed line in Fig. 9) as it would appear in this normalization if the change in slope occurred at 2.1 f_p.

The break in slope near 2.1 f_p is intriguing because some authors, notably Forristall (1981), report a break in slope from f^{-4} (equivalent to $k^{-5/2}$) to f^{-5} (or k^{-3}) behavior in observed spectra, and others, e.g., Mitsuyasu, et al. (1980) and Donelan, et al. (1985), do not. Forristall (1981), in a study of hurricane waves in the Gulf of Mexico, cast his observations in terms of normalized frequency $\tilde{f} = u_* f/g$, and found a break in slope near $\tilde{f} =$ 0.0275. When we cast the Currituck Sound observations in terms of $\tilde{f}$, we find a break in slope near $\tilde{f} =$ 0.0200, which suggests a dissimilarity of the two data sets in this form of scaling, possibly owing to differences between the very young Currituck Sound waves and the more fully evolved waves examined by Forristall (1981). To follow this thought, we cast data from NDBC buoys 41001 and 46034 (used in Fig. 2 and chosen for steadiness in wind speed and direction as well as narrowness of spectral peaks to reduce the probability of coexisting swell) in the compensated form used in Fig. 9. The result is shown in Fig. 10, where, amid greater data scatter than in Fig. 9, there appears to be a deviation from $k^{-5/2}$ behavior for $f > 2.9 f_p$. The dashed line in Fig. 10 indicates a k^{-3} behavior intersecting the equilibrium-range curve at 2.9 f_p. One difference between Fig. 9 and Fig. 10 is that (in the mean) the spectral peak exceeds the equilibrium range curve by a greater amount for the Currituck Sound data than for the NDBC data. Another difference is that the transition frequency between the two power-law behaviors is lower for the Currituck Sound data than for the NDBC data. This suggests that the bandwidth of the equilibrium range may depend on the stage of wave development, a condition that can be characterized by wave age.

To see if such a pattern exists within the suite of Currituck Sound and NDBC observations, we stratified those spectra in classes of inverse wave age u_l / c_p, which arises from the success (discussed in Section 2) of $\left(u_l^2 c_p\right)^{1/3}$ as an equilibrium-range velocity scale and the consequent corresponding inverse age $\left(u_l^2 c_p\right)^{1/3}/c_p = \left(u_l/c_p\right)^{2/3}$ that

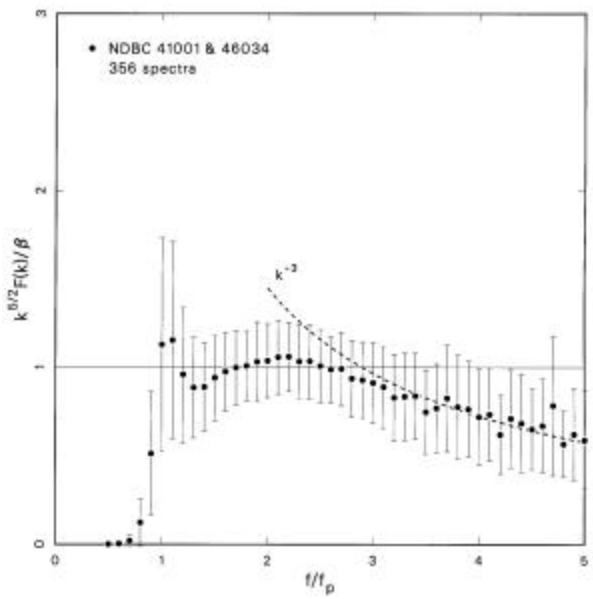

Fig. 10. Means (symbols) and standard deviations (error bars) of 356 sample spectra from NDBC buoys 41001 and 46034 normalized by equilibrium-range scales.

can be represented simply by u_l / c_p. We used eight stratification bins for the NDBC data and seven for the Currituck Sound data, with bin boundaries selected to contain representative numbers of samples and to be common for both data sets where the sets had similar inverse wave ages.

Fig. 11 shows the averaged spectra within our stratification classes, with classes representing 'old' waves at the bottom of the figure all being from the NDBC data and classes representing 'young' waves at the top of the figure all being from the Currituck Sound data. There are three classes from each set with common ranges of wave age. The broad pattern indicated by Fig. 11 is that the class-averaged spectra deviate from the horizontal equilibrium-range line at much higher f/f_p for old waves than for young waves. The indication is that there is a break in slope at $f/f_p > 3$ for the oldest waves, but the break occurs at $f/f_p \cong 2$ for the youngest waves.

Close examination of Fig. 11 indicates that the structures of compensated spectra in overlapping classes from the two sets are not identical, especially in the region of the spectral peak. This condition may arise owing to our use of the Charnock relation alone to estimate u_* from measured wind speed, when it is well known that atmospheric stratification can modify drag coefficients for low to moderate wind speeds. As defined by (5), u_l is a strong function of u_*, so we may have misestimated somewhat the wave ages of some of our spectra and thus affected the structure of our class averages. Such errors would not shift class members by more than one or two classifications, however, so the broad pattern indicated by Fig. 11 is unchanged.

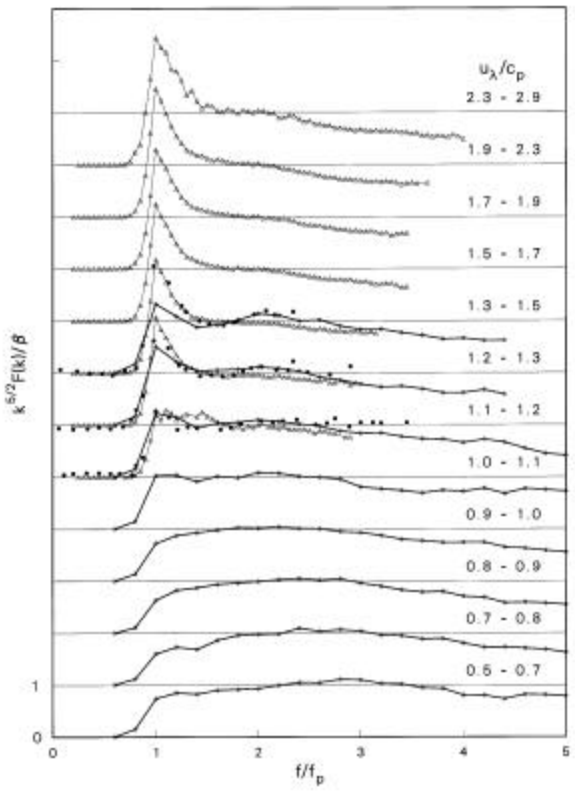

Fig. 11. Currituck Sound mean spectra in classes of equilibrium-range inverse wave age.

The solid dots in Fig. 11 are data (extracted by hand) representing three age classes from Fig. 12 of the well-known paper by Donelan, et al. (1985), who classed their results with an age given by u_{10}/c_p. Those class averages are imposed on our classed data not by inverse age, but by the general extent to which the spectral peaks exceed the equilibrium-range curve (the close alignment of spectral peak values between the two sources is fortuitous), and so may be only approximately correctly placed. The point of this exercise is to show that their results for young field data extend to an f / f_p that is too low to detect a break in slope. Thus, our results do not conflict with theirs. Note that the three age classes of data from Donelan, et al. (1985) not used here include one case of older field data, which is consistent with our assumed pattern, and two cases of laboratory data, which do not agree with our pattern, but which may not be representative of open-water data.

We performed a (very) qualitative test of the suggested pattern by assuming that the class-averaged compensated spectra in Fig. 11 consist of an equilibrium range with $\hat{F}\left(\hat{f} = f/f_p\right) = k^{5/2}F(k)/b = 1$ for $1.5 < \hat{f} \le \hat{f}_m$ and a k^{-3} range for which $\hat{F}\left(\hat{f}\right) = \hat{f}_m \hat{f}^{-1}$ for $\hat{f} \ge \hat{f}_m$ with the transition frequency $\hat{f}_m$ a function of u_l/c_p. We isolated a probable $\hat{f}_m$ by allowing it to vary until we found a

minimum in the sum square error of the two models, as defined by

$$\sum_{1.5}^{\hat{f}_m}\left[\hat{F}\left(\hat{f}\right)-1\right]^2+\sum_{\hat{f}_m}^{\hat{f}_2}\left[\hat{F}\left(\hat{f}\right)-\hat{f}_m\hat{f}^{-1}\right]^2,$$

where $\hat{f}_2$ is the highest frequency within a class.

Fig. 12 shows the resulting $\hat{f}_m = f_m / f_p$ as a function of u_l / c_p for the fifteen classes shown in Fig 11. The result is certainly not conclusive, but is suggestive of a pattern wherein the break in slope shifts to a higher multiple of the spectral peak frequency as wave age increases. The general trend of these results suggests that the pattern is worthy of further study, especially using a broader suite of data with very well resolved high frequency spectral tails. The indicated trend may account qualitatively for findings by various investigators of the existence or location of a break in slope, given its possible age- and f_p-dependence, in conjunction with details of spectral sampling. For example, Mitsuyasu, et al. (1980) show two specific examples of spectra with no break in slope up to $f / f_p = 3$. Estimates (from their tables and figures) of u_l / c_p are less than 0.5 in both cases, which makes their observations consistent with our Fig. 12.

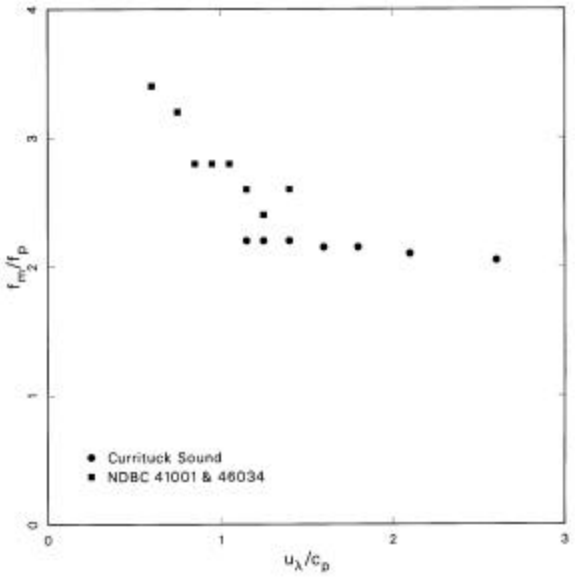

Fig. 12. Slope transition frequency as a function of inverse wave age.

A possible cause of this behavior is that, as mentioned in Section 2, the net non-linear flux through the equilibrium range tends to vary as b^3. For very young (small- b) waves, the equilibrium range may be less well developed than for older waves. Investigation of this process requires integration of the wave evolution equation with all source terms active, i.e., there is an integral time scale associated with the non-linear energy flux that we only loosely characterize with inverse wave age. Numerical work, in conjunction with some better field data, will help determine if our conjecture has verity.

4.2 Consideration of Lake George Data

Our original intent was to replicate in part the Lake George observations, so it is of interest to examine those data in the same normalization as is used in Fig. 9. Fig. 13 shows the Lake George data used by Resio, et al. (2004), where, like the Currituck Sound data, we used only those cases satisfying $u_{10} > 5$ m/s and for which the winds came from the long axis or far side of the lake.

The data shown in Fig. 13 are different in detail from the data shown in Fig. 9. The range of observed frequencies is higher for Lake George, extending here to more than 15 f_p. In the conventional equilibrium range of frequencies from 1.5 f_p to 3 f_p, there is no region of constant compensated energy density, but rather a peak in the vicinity of 2 f_p. Because these waves have propagated from mid-lake water depths of about 2 m to local depths of 0.6 m to 1.1 m, a Fourier energy peak at 2 f_p is likely a signature of shoaling waves.

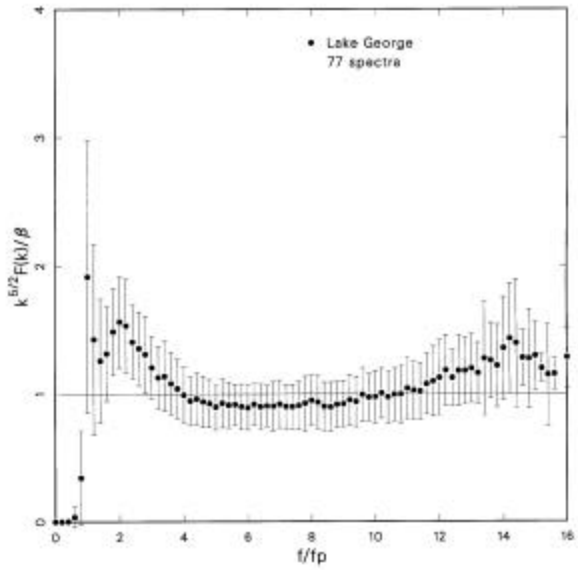

Fig. 13. Means (symbols) and standard deviations (error bars) of 77 normalized wave-number spectra from Lake George.

Interestingly in Fig. 13, there is a range of approximately constant compensated energy density for frequencies from about 4 f_p to about 9 f_p, well beyond the conventional equilibrium range of frequencies. The compensated values in this range do not equal one because we used data for all $f \geq 2.5 f_p$ in estimating b. Some points have elevated values relative to the apparent equilibrium range, so b is slightly over-estimated. Normalization by this over-estimated b results in compensated spectra slightly less than unity. The breadth in frequency of the apparent

equilibrium range seems curiously large, but this may be a consequence of shallow depth. Resio, et al. (2001) note that non-linear interaction rates are expected to increase significantly (relative to deep water) for $k_p h$ less than about 1.2. For the Lake George data used here, the expected $k_p h = 1.21 \pm 0.57$, whereas for Currituck Sound, $k_p h = 2.48 \pm 0.43$. Thus, non-linear interactions are likely to be stronger in the Lake George environment than in Currituck Sound. That a more dominant S_{nl} results in a broader equilibrium range is consistent with our observations associated with Fig. 12, but it is not obvious why spectral levels would continue to follow the equilibrium scale given by (6), especially in the possible presence of shoaling effects in addition to the effects of S_{in} and S_{ds}.

Another difference between the two data sets is there is no spectral decay evident in the Lake George data at frequencies higher than the apparent equilibrium range. In fact, the spectra increase relative to a $k^{-5/2}$ behavior. It is not clear why this behavior exists. These data differ in detail from our Currituck Sound observations, so numerical and replicate field studies may be required to account for their behavior.

5. DIRECTIONAL DISTRIBUTION FUNCTIONS

To characterize the directional nature of the whole set of 649 frequency-direction spectra used in this study, we rotated each directional distribution function $D(k,q)$ so that its zero direction aligned with the wind direction $D(k,q-q_w)$, and the wave number coordinate was expressed in discrete bins relative to k_p, thus obtaining a set of $D(k/k_p,q-q_w)$. For each discrete $(k/k_p,q-q_w)$ bin, we then have a number of samples from which we can construct mean $\overline{D}(k/k_p,q-q_w)$ and standard deviation $s_D(k/k_p,q-q_w)$ normalized directional distribution functions representative of our data. Note that we eliminated from the average any part of any spectrum that violated our noise floor constraint, so the high-wave-number parts of our statistical distributions are based on fewer samples than those near the spectral peaks. Figs. 14 and 15 illustrate $\overline{D}$ and s_D, respectively. Fig. 16 is a contour plot of $\overline{D}$.

The mean directional distribution function found here has some of the well-known features deduced or observed by other researchers, including a narrow, single-mode distribution near the spectral peak, and a broad, clearly bimodal distribution at higher frequencies. These results are qualitatively similar to observations in Lake George reported by Young, et al. (1995), except that the present results seem better resolved, owing probably to the use of a nine-element array (instead of seven), the IMLE algorithm (instead of MLE) and the use here of a great number of

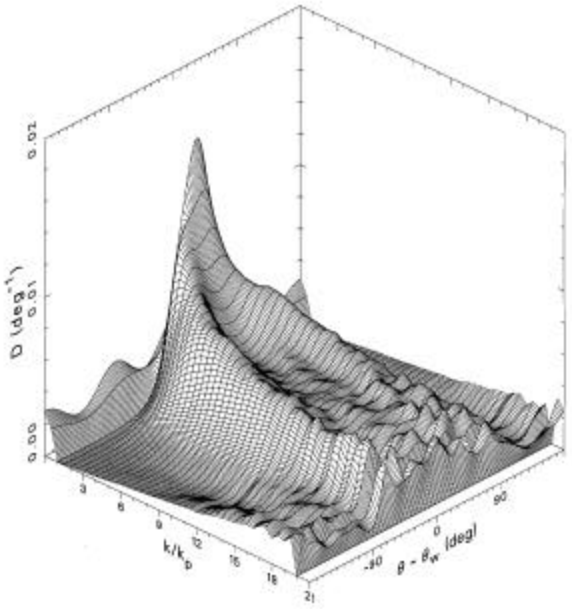

Fig. 14. Mean normalized directional distribution function from 649 Currituck Sound observations.

observations in the average. In a reasonable analysis, Young, et al. (1995) deduce from numerical studies that the bimodal structure owes to the influence of S_{nl}. It is interesting that in the present data there is clear evidence of bimodal structure at $k/k_p = 16$ (or $f/f_p = 4$), and some evidence (see Fig. 16) that the bimodality extends to the highest wave numbers for which we could perform statistics,

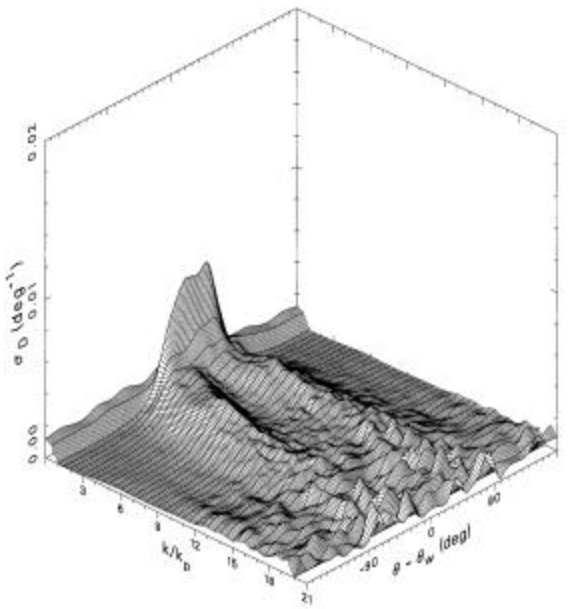

Fig. 15. Standard deviation of the set of directional distribution functions observed in Currituck Sound.

though the downwind part of the directional distribution is much whiter at the highest wave numbers. In contrast, the part of the mean one-dimensional spectrum (Fig. 9) that we call the equilibrium range (where, supposedly, the sum effect of sources scales with S_{nl}) extends only to $f/f_p \cong$ 2.3 or $k/k_p \cong 5.9$. If S_{nl} continues to be influential at much higher frequencies, the transition between dominance

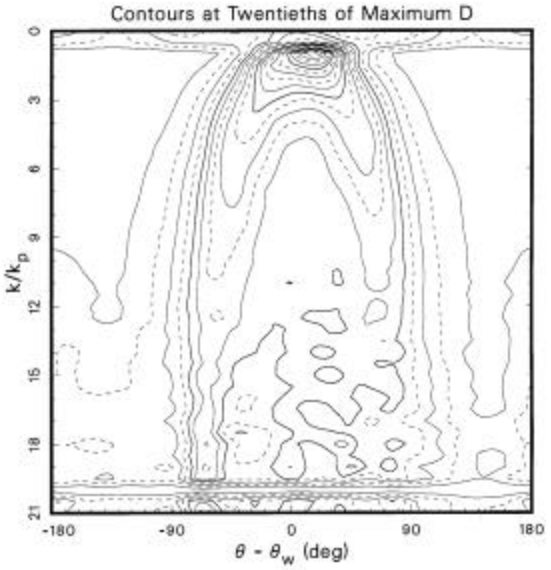

Fig. 16. Contours of mean directional distribution function shown in Fig. 14.

of the various source terms must be quite subtle. The whitening of the downwind directional distribution in Fig. 14, which may be a signature of S_{ds}, appears to begin near $k/k_p = 12$. It should be quite enlightening to investigate numerically (an obvious next step) what kinds of source terms are necessary to replicate this behavior.

The evident broadening of the directional distribution at wave numbers below the spectral peak in Fig. 14 is artificial. Within the discrete k/k_p bins used in that figure, the low-wave-number bins include estimates for waves that are longer than the array can resolve, so the results are not good.

In directions satisfying $|q - q_w| > 90$ deg in Fig. 14, there is evidence of high-frequency waves traveling upwind, a condition we did not expect in open water. We assumed that this signal owed to short waves reflecting from the tower and gauge cage of our instrumented sled. Because such waves would not be part of a natural wind sea, and would contaminate our estimates of the one-dimensional spectra, we based the spectra used in Section 4 on the downwind parts of the frequency-direction spectra in accordance with (13).

That the mean directional distribution is representative of its constituent members is suggested by the standard deviation of the set shown in Fig. 15. s_D is generally less than $\overline{D}$ over the whole domain, and especially in the downwind directions at wave numbers just above the spectral peak. Larger s_D occur in the vicinity of the spectral peak and the immediate bimodal tails, and lie beneath these features. This suggests that there may be subtle variations in the structures of constituent directional distributions, but that the pattern shown in Fig. 14 is fairly representative.

To examine variations in structure of the directional distribution functions, we stratified the 649 observations into the same seven equilibrium-range inverse age classes used in Fig. 11 for the one-dimensional spectra, and averaged the members of each class using the same method described above for $\overline{D}$. Space precludes showing results for all classes, but we show two classes in Fig. 17, one for 'old' waves $1.2 < u_1/c_p < 1.3$ (an average of 42 cases) and one for 'new' waves $1.9 < u_1/c_p < 2.3$ (based on 77 cases). The two distributions in Fig. 17 have narrow single-mode peaks and bifurcated high-frequency tails in general similarity with the overall mean of Fig. 14 (they are plotted on the same scale as Fig. 14, but are truncated owing to our noise-floor constraint). The main difference between the two distributions is that the bifurcation peaks of the younger directional distribution span a broader range of direction than those of the older distribution. This characteristic may be important. Our observations are limited to a small range of inverse ages and are related only to small waves within much wider continua of both wave age and wave height. If bifurcation separation in the spectral tails detectably decreases with increasing wave age in our limited observations, it is possible that for very old waves, the bifurcation disappears, or at least narrows considerably. At the opposite asymptote, extremely young waves may have very broad bimodal distributions. If the non-linear fluxes are negligibly small on this asymptote, the system may shift to a very different balance of source terms.

Because three-dimensional plots can be illusory, we attempt to clarify the apparent age dependence of the bifurcation separation by considering directional cross-sections through our seven class-averaged distributions at a fixed k/k_p. For each distribution, we averaged (i.e., smoothed) the directional distribution estimates over the five wave-number bins spanning $7 \le k/k_p \le 9$, with the latter limit simply being the highest frequency for which we had averages in our oldest age class. Fig. 18 shows the seven resulting distributions. There, we see a rather smoothly decreasing separation of the directional peaks from about 130 deg for the youngest class (uppermost curve) to about 110 deg for the oldest class (lowermost curve). The gradation is not huge, but neither is our range of ages, so asymptotic extremes may be significant.

Related to this, we note that Ewans (1998) in a study of fetch-limited waves in 110-m water depth near New Zealand was able to distinguish directional modal separation for waves of 0.5 m to 4.2 m height and with inverse wave ages

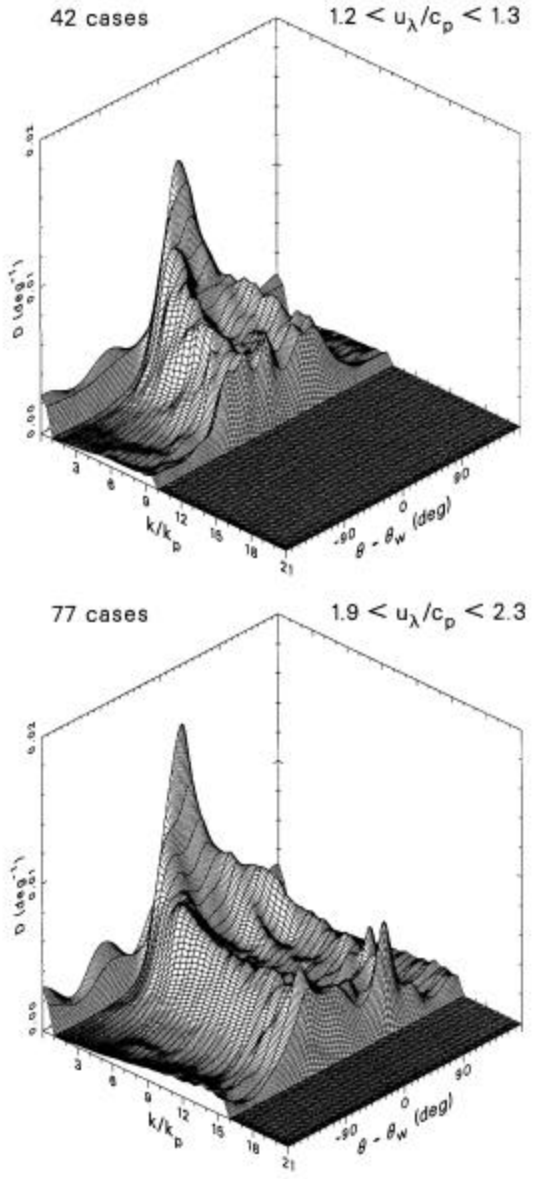

Fig. 17. Mean directional distributions in two wave age classes: 'old' waves (upper image) and 'young' waves (lower image).

u_{10}/c_p ranging from 0.7 to 1.4. These waves are older than our waves, which have u_{10}/c_p ranging from 1.5 to 4.1. In a scatter plot of modal separations in terms of f/f_p based on 77 spectra, Ewans (1998) finds a separation range of roughly 90 deg to 105 deg at $f/f_p = 2.8$, or $k/k_p = 8$, which is near the scale represented in Fig. 18. Ewans (1998) does not note a distinction among the wave ages represented by his observations, but his waves are older than ours, and his range of modal separations is slightly narrower than the range suggested by Fig. 18. Furthermore, at $f/f_p = 4$

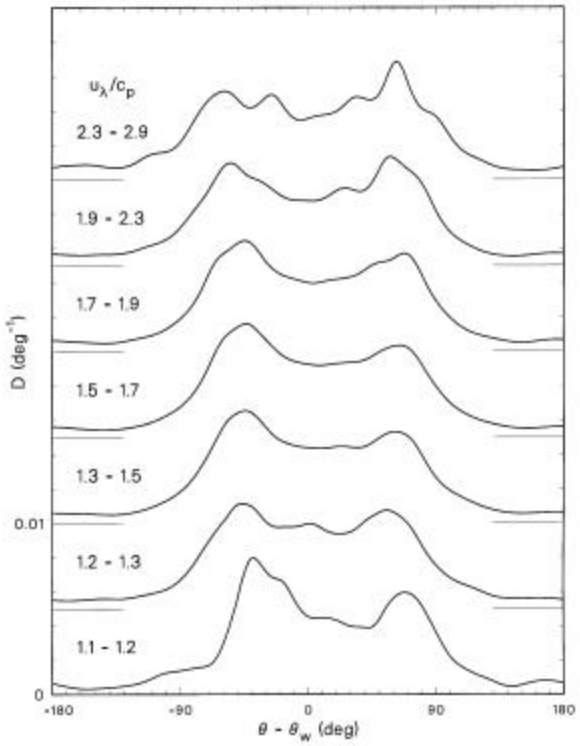

Fig. 18. Smoothed directional sections through six class-averaged directional distributions near $k/k_p = 8$.

($k/k_p = 16$), Ewans (1998), near his highest reported f/f_p, finds separations of about 105 deg to 120 deg, which is narrower than the ~130 deg we see in our overall mean distribution of Fig. 16. This suggests that our results may, indeed, be part of continuum of distributions that narrow with increasing wave age.

The variation in directional behavior also extends into the region near the spectral peak, which we identify here as that part of the spectrum for which $0.5 \le k/k_p \le 2.5$, or, approximately $0.7 \le f/f_p \le 1.6$. Using a smaller increment of k/k_p than used in Figs. 16 and 17 within which to accumulate bin averages, we are able to elucidate some of the directional structure near the spectral peak.

Fig. 19 shows the mean directional distribution function that results from using all 649 of our observations. The distribution at the spectral peak has a single mode, as expected, and the distribution surface clearly begins to split into a bimodal form near $k/k_p = 2$, or $f/f_p \cong 1.4$. This observation differs from results given by Young, et al. (1995). They indicate that the directional distribution function retains a single mode for frequencies up to $f/f_p = 1.5$. However, not all of our directional distribution functions are clearly bimodal at this dimensionless

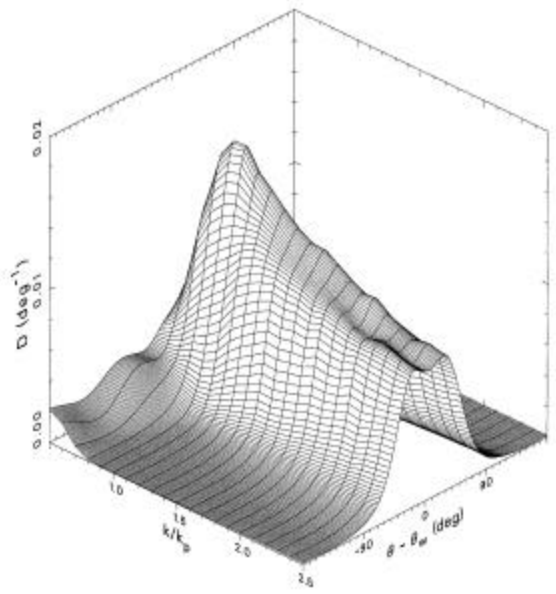

Fig. 19. Bin-averaged directional distribution function near the spectral peak based on all 649 Currituck Sound observations.

frequency. When we stratify and average our observations in the seven equilibrium-range inverse age classes that we used for the one-dimensional spectra, we find an age-related variation in directional structure.

Fig. 20 shows mean directional distributions for two of these classes, one 'old' (upper panel) and one 'young' (lower panel), corresponding to the same classes shown in Fig. 17. Fig. 20 indicates that for both age classes, the directional distribution has a single mode at the spectral peak, but that there is a clear variation in structure at the higher frequencies. For what we call a young sea, there is clear bimodality through a range of frequencies that begins very near to the spectral peak, with the bifurcation point near $k/k_p = 1.4$, or $f/f_p = 1.2$. In contrast, the directional distribution function for the older sea is less clearly bimodal. There appears to be partial bifurcation at some of the higher frequencies, but the pattern is far less systematic than that of the younger sea. In this case, one might possibly model the directional distribution at $f/f_p = 1.5$ as a single-mode function, as was done by Young, et al. (1995).

In any case, the structure of the older directional distribution function is clearly different from that of the younger case, with the latter splitting into two distinct modes at frequencies nearer the spectral peak. This is qualitatively consistent with our earlier observation that directional distributions tend to narrow with increasing age, and is probably related to our speculation that the frequency band of the equilibrium range increases with overall wave age.

We note that members of our data set are all samples of young waves. The variations in spectral shape and directional structure we observe in our data may owe simply to subtle variations in the effects of the various source terms in the initial stages of wave growth. However, the trends we

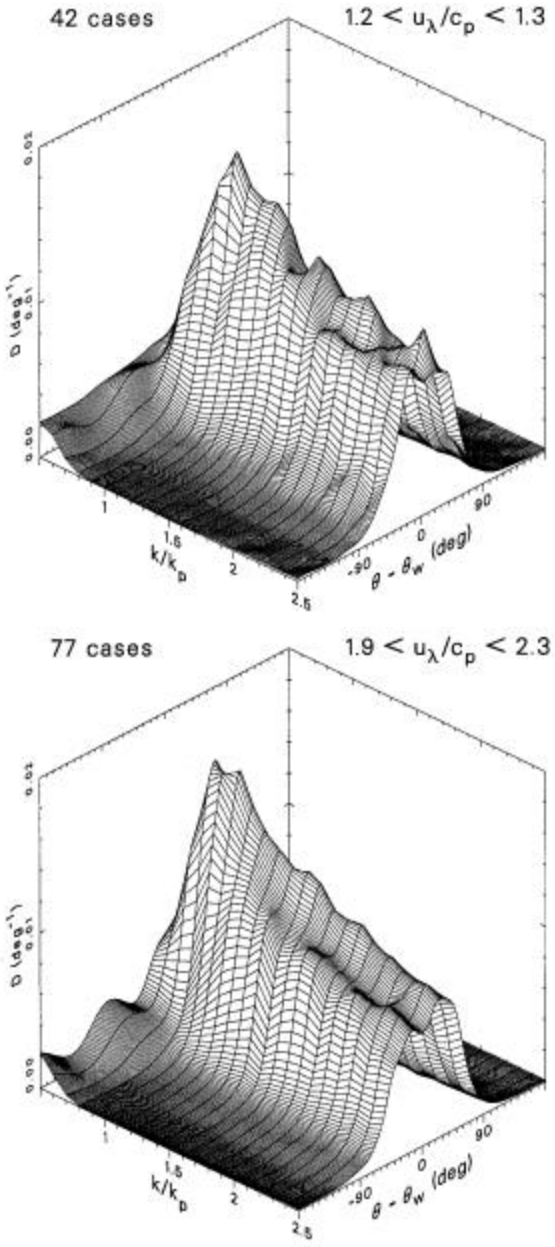

Fig. 20. Mean directional distribution functions in the vicinity of the spectral peak for 'old' waves (upper image) and 'young' waves (lower image) from two wave-age classes.

see in our young data are qualitatively consistent with results reported by Ewans (1998) for somewhat older ocean waves. This suggests that there is a continuum in the net effects of the various source terms in wind waves that gives rise to frequency-direction spectra with structures in their energy distributions that depend at least on wave age.

5. SUMMARY

Motivated by what appeared to be curious behavior in the scales of Lake George data relative to oceanic data, we

conducted a field study of directional wind wave behavior in Currituck Sound, North Carolina. In the one-dimensional spectra from that site, we see evidence of both an equilibrium range following a $k^{-5/2}$ behavior and, at higher frequencies, another range following a k^{-3} behavior. We find the bandwidth of the equilibrium range in our data to be narrower than the conventional range of $1.5 < f/f_p < 3$, but, when compared to data from two NDBC gauges, it appears that the equilibrium-range bandwidth is a function of and increases with wave age. The average two-dimensional directional distribution function, based on 649 observations, has a narrow, single-mode peak and clear directionally bimodal structure at higher frequencies, in agreement with observations by Young, et al. (1995). Stratification of our directional observations in classes of wave age show a subtle change in shape, with broader distributions for young seas and narrower distributions for older seas, suggesting an age-related variation in directional spectral structure, at least for our young waves. The trend indicated by our results is qualitatively consistent with observations by Ewans (1998), who finds even narrower distributions for his older data.

These variations in directional spectra suggest that the net effect of the source terms varies as waves evolve. Our observations indicate the results of those effects, but serve only as clues about the nature of the source terms. The subtle variations we see occur at high frequencies where there is little energy, and by that measure may not be of much import. However, given that the growth and evolution of wave spectra depend on energy fluxes through all frequencies, it may be quite important to discern details of spectral structure at frequencies well above the spectral peak. It remains to obtain independent observations that will verify the patterns we see in our data, and to characterize the detailed physics of wind wave source terms such that models can replicate this behavior.

Acknowledgments. The Currituck Sound expedition would not have been possible without the intrepid and frequently brilliant contributions of Brian Scarborough and Kent Hathaway, and the stalwart efforts of Bill Grogg, Dan Freer, Ray Townsend and Mike Leffler, all of the FRF. Many thanks to Ian Young and Alex Babanin for providing the Lake George data used in this study.

REFERENCES

Babanin, A. V., I. R. Young and M L. Banner, 2001: Breaking probabilities for dominant surface waves on water of finite constant depth. *J. Geophys. Res.*, **106**, 11,659-11676.

Charnock, H., 1955: Wind stress on a water surface. *Q. J. Roy. Met. Soc.*, **81**, 639-640.

Davis, R. E. and L. A. Regier, 1977: Methods for estimating directional wave spectra from multi-element arrays. *J. Mar. Res.*, **35**, 453-477.

Donelan, M. A., J. Hamilton and W. H. Hui, 1985: Directional spectra of wind-generated waves. *Phil. Trans. R. Soc. Lond.* **A**, **315**, 509-562.

Ewans, K. C., 1998: Observations of the directional spectrum of fetch-limited waves. *J. Phys. Oceanogr.*, **28**, 495-512.

Forristall, G. Z., 1981: Measurements of a saturated range in ocean wave spectra. *J. Geophys. Res.*, **86**, 8075-8084.

Hasselmann, K., 1961: On the nonlinear energy transfer in a gravity-wave spectrum. Part I. General Theory. *J. Fluid Mech.*, **12**, 481-500.

Hert erich, K. and K. Hasselmann, 1980: A similarity relation for the non-linear energy transfer in a finite-depth gravity-wave spectrum. *J. Fluid Mech.*, **97**, 215-224.

Kitaigorodskii, S. A., 1983: On the theory of the equilibrium range in the spectrum of wind-generated gravity waves. *J. Phys. Oceanogr.*, **13**, 816-827.

Long, C. E., 1995: Directional wind wave characteristics at Harvest Platform. Tech. Rep. CERC-95-4, U.S. Army Engineer Waterways Experiment Station, Vicksburg, MS, 182 pp.

Mitsuyasu, H., F. Tasai, T. Suhara, S. Mizuno, M. Ohkusu, T. Honda and K. Rikiishi, 1980: Observation of the power spectrum of ocean waves using a cloverleaf buoy. *J. Phys. Oceanogr.*, **10**, 286-296.

Pawka, S. S., 1983: Island shadows in wave directional spectra. *J. Geophys. Res.*, **88**, 2579-2591.

Resio, D. T., 1987: Shallow-water waves, I: Theory. *J. Waterway, Port, Coastal and Ocean Eng.*, **113**, 264-281.

_____ and W. Perrie, 1989: Implications of an f^{-4} equilibrium range for wind-generated waves. *J. Phys. Oceanogr.*, **19**, 193-204.

_____ and _____, 1991: A numerical study of nonlinear energy fluxes due to wave-wave interactions. Part 1. Methodology and basic results. *J. Fluid Mech.*, **223**, 603-629.

_____, V. R. Swail, R. E. Jensen and V. J. Cardone, 1999: Wind speed scaling in fully developed seas. *J. Phys. Oceanogr.*, **29**, 1801-1811.

_____, J. H. Pihl, B. A. Tracy and C. L. Vincent, 2001: Nonlinear energy fluxes and the finite depth equilibrium range in wave spectra. *J. Geophys. Res.*, **106**, 6985-7000.

_____, C. E. Long and C. L. Vincent, 2004: Equilibrium-range constant in wind-generated wave spectra. *J. Geophys. Res.*, **109**, C01018, doi: 10.1029/2003JC001788.

Toba, Y., 1972: Local balance in the air-sea boundary processes. I. On the growth process of wind waves. *J. Oceanogr. Soc. Jap.*, **28**, 109-121.

_____, 1973: Local balance in the air-sea boundary processes. III. On the spectrum of wind waves. *J. Oceanogr. Soc. Jap.*, **29**, 209-220.

Tracy, B. A. and D. T. Resio, 1982: Theory and calculation of the nonlinear energy transfer between sea waves in deep water. Wave Information Study Report 11, U. S. Army Engineer Waterways Experiment Station, Vicksburg, MS, 47 pp.

Webb, D. J., 1978: Nonlinear transfer between sea waves. *Deep-Sea Res.*, **25**, 279-298.

Young, I. R., L. A. Verhagen and M. L. Banner, 1995: A note on the bimodal directional spreading of fetch-limited wind waves. *J. Geophys. Res.*, **100**, 773-778.

Zakharov, V. E. and N. N. Filonenko, 1966: Energy spectrum for stochastic oscillations of the surface of a liquid. *Dokl. Akad. Nauk SSSR*, **160**, 1292-1295.